Biosensors and Bioelectronics 42 (2013) 326–331

Contents lists available at SciVerse ScienceDirect

Biosensors and Bioelectronics

journal homepage: www.elsevier.com/locate/bios

Label-free DNA microarray bioassays using a near-field scanning microwave microscope

Kiejin Lee [a,*], Arsen Babajanyan [a], Harutyun Melikyan [a], Chongchel Kim [a], Seungwan Kim [a], Jungho Kim [b], Jung-Ha Lee [b], Barry Friedman [c], Rastislav Levicky [d], Sergey Kalachikov [e]

[a] Department of Physics and Basic Science Institute for Cell Damage Control, Sogang University, Seoul 121-742, Republic of Korea
[b] Department of Life Science and Basic Science Institute for Cell Damage Control, Sogang University, Seoul 121-742, Republic of Korea
[c] Department of Physics, Sam Houston State University, Huntsville, TX 77341, USA
[d] Department of Chemical and Biological Engineering, Polytechnic Institute of New York University, NY 11201, USA
[e] Columbia Genome Center, Columbia University, NY 10032, USA

ARTICLE INFO

Article history:
Received 14 August 2012
Received in revised form
5 October 2012
Accepted 8 October 2012
Available online 26 October 2012

Keywords:
DNA bioassay
Oligonucleotide microarrays
Microwave microscope

ABSTRACT

A near-field scanning microwave microscope (NSMM) is used to readout and visualize homemade 10-mer oligonucleotide microarrays and an Agilent 60-mer DNA microarray as a realistic test of NSMM applicability to multiplexed sequence analysis. Sensitive characterization of DNA coverage and high resolution mapping of DNA spots in the microarray were realized by measuring the change of microwave reflection coefficient (S_{11}) at about 4 GHz operating frequency. Hybridization between target (free) and capture (immobilized) sequences leads to changes in the microwave reflection coefficient, which were measured by the NSMM. These changes are caused by hybridization-induced modification of the dielectric permittivity profile of the DNA film. The dynamic range based on analysis of the 10-mer microarrays is over 3 orders of magnitude with the detection limit estimated below 0.01 strands/μm^2. The NSMM method should be readily capable of detecting target coverages down to 98% of probe coverage. We also directly image the patterned DNA microarray by NSMM with a 2 μm resolution. The complementary optical image of the DNA microarray visualized by using a relative fluorescent intensity metric agrees well with the NSMM results.

1. Introduction

The DNA microarray format is a powerful tool that allows sequence-analysis of RNA and DNA mixtures in a highly parallelized fashion. Current methods of detection have mainly focused on optical detection including fluorescence-labeled oligonucleotides with dye, quantum dot, or enhanced absorption of light by oligonucleotide-modified gold nanoparticles (Wang and Li, 2011; Hanai et al., 2006; Lamartine, 2006). Fluorescence is extremely sensitive, allowing single molecule detection (Zheng et al., 2007; Ray et al., 2010). Nanoparticle labels to detect DNA have also proved very useful (Cao et al., 2008; Son et al., 2007; Qi et al., 2009), providing a mechanism that transduces and amplifies specific DNA binding events to detectable signals. For example, DNA strands with a complementary sequence to that of target DNA can be chemically linked to gold nanoparticles and optical, electric, magnetic or other properties can be used to detect the binding of target molecules (Ryu et al., 2010; Postma, 2010; Lin et al., 2009).

However, ideal microarray imaging would retain sufficiently high sensitivity without relying on chemical labeling or expensive instrumentation (Ozkumur et al., 2010). Such label-free diagnostics are attractive as they simplify sample preparation, decrease assay costs and eliminate potential artifacts from label instability or perturbation of assay thermodynamics (Baur et al., 2010; Zhang et al., 2010; Zhu et al., 2009; Maruyama et al., 2009). A number of label-free approaches for direct measurement of various analytes have been described based on optical, impedance, charge, mass, and electrochemical transduction (Dolatabadi et al., 2011; Pei et al., 2001; Elson, 2007; Ziolkowski et al., 2010; Shervedani et al., 2006). These methods promise to offer sensitivity, selectivity, and lowered costs for analysis of DNA sequences through surface hybridization.

The design, imaging performance, and applications of near-field scanning microwave microscopy (NSMM) for noninvasive characterization of electrical properties of conducting and dielectric materials have been previously described (Knoll et al., 1997; Abu-Teir et al., 2001; Kim et al., 2003; Lim et al., 2008). The changes in intrinsic impedance and material characteristics (electrical conductivity, dielectric permittivity, magnetic permeability,

* Corresponding author. Tel.: +82 2 705 8429; fax: +82 2 715 8429.
E-mail address: klee@sogang.ac.kr (K. Lee).

0956-5663/$ - see front matter © 2012 Elsevier B.V. All rights reserved.
http://dx.doi.org/10.1016/j.bios.2012.10.027

volumetric and thin film properties, etc.) of various materials were investigated by NSMM by measuring the microwave reflection coefficient S_{11}. The reflection coefficient depends on the complex dielectric permittivity profile ε across the surface being probed. Difference in ε for DNA and substrate, for example, will manifest in shifts in resonance frequency f_r and reflection coefficient amplitude S_{11}, and can be mathematically modeled by transmission line theory within a material perturbation approach, assuming near-field dipole–dipole interactions (Bhushan, 2011; Ohtsu, 1998; Pozar, 1990). Physically, the dielectric permittivity of a DNA-modified microarray spot is expected to depend on length and surface coverage of the strands, on hybridization state and distribution of the molecules (e.g. single oligonucleotide probe vs. double-stranded, ordered vs. disordered) and presence of other species on the surface including, most prominently, physisorbed water (Kim et al., 2011). In this report, the DNA spots on microarrays were imaged by measuring the local microwave reflection coefficient S_{11} at the resonance frequency, $f_r = 3.98$ GHz.

In previous reports, we demonstrated this approach for label-free, high-sensitivity imaging of n-alkylthiol and DNA prototype arrays (Kim et al., 2011; Friedman et al., 2005). In this paper, we demonstrate that NSMM is able to measure the surface coverage of analyte species at sensitivities comparable to conventional commercial fluorescence bioassay devices. The NSMM approach does not require functionalization of DNA strands with fluorescent dyes, redox couples, nanoparticles, or other labels. The technique therefore provides a very convenient and straightforward approach to multiplexed analysis of DNA sequences while maintaining the high sensitivity required for such applications.

2. Materials and methods

2.1. Sample preparation

DNA sample 1: Custom made DNA arrays with variable coverage were prepared for characterizing the NSMM detection response as a function of DNA coverage. 10-mer HPSF-purified homopolymers (A_{10}, T_{10}, C_{10}, G_{10}) were purchased from MWG Biotech (Eurofins MWG Operon, AL). Arrays of these oligonucleotides were printed on SigmaScreen microarray slides with an aminopropyltriethoxysilane coating, using an Affymetrix GMS 417 spotter (Affymetrix, CA). Spotting was performed from deionized water at six concentrations obtained by 10-fold serial dilutions, starting from 0.005 strands/μm^2 (i.e. spotting concentrations of 0.005, 0.05, 0.5, 5, 50 and 500 strands/μm^2). Each dilution of each oligonucleotide was printed 12 times, with three spots printed with each of the four pins on the GMS 417. The spots were allowed to dry, with no further processing applied, followed by NSMM imaging. Slides were not washed so as to preserve the number of strands printed. Deionized water was used for printing in order to minimize nonvolatiles that might co-deposit with the DNA. Area-averaged oligonucleotide coverages σ were estimated from the microarray spot radius $R \approx 70\ \mu m$, the printing concentration C, and the approximate volume $V \approx 1$ nL transferred using $\sigma = VCN_A/\pi R^2$, where N_A is Avogadro's number. Estimated coverages range from $\sim$0.005 strands/μm^2 on the low end (0.00011 nM printing solution) to $\sim$500 strands/μm^2 for the highest printed concentration (11 nM). The intention of using oligonucleotides comprised of the same residue repeat was to determine whether selection of base (A, T, C, G) influences the strength of the NSMM response. In contrast to methods employing covalent bonding between the microarray and printed DNA, the DNA for these model studies were simply physisorbed to the positively charged microarray surface. After drying of the printed spots no further processing steps (including washing) were used so as to not alter coverage of the deposited strands.

DNA sample 2: Total RNA was isolated from the sarcoma-derived human cell line GBS6 using TRIzol reagent (Invitrogen), labeled using Agilent low RNA input fluorescent linear amplification kit (Agilent, CA) and hybridized to human whole genome 44k 60-mer oligonucleotides microarray chips (Agilent, CA) using one-color (red) gene expression system following the manufacturer's instructions. The integrity of RNA samples and the extent of DNase digestion during the labeling procedure were monitored with the Agilent 2100 Bioanalyzer (Agilent, CA). All steps, including imaging of the hybridized microarray, were performed with Agilent Technologies instrumentation. For details see also Van Schothorst et al. (2007). We generated fluorescent cRNA (complimentary RNA) with a sample input RNA (GBS6 RNA) for one-color processing using Agilent's low input quick amp labeling kit (Agilent Technologies) according to the manufacturer's instruction. This method uses T7 RNA polymerase, which simultaneously amplifies target material (total RNA isolated from GBS6 cells) and incorporates cyanine 3-labeled CTP. Thus, it is impossible to tell the exact RNA sequences that are used for this experiment. We guess the total RNA sequences from the GBS6 cells were amplified. According to the literatures published by Agilent Technologies, amplification is typically at least a 100-fold from total RNA to cRNA with the use of this kit. We also used an Agilent 60-mer whole human genome microarray for the experiments in this study. According to the manufacturer (Van Schothorst et al., 2007), this microarray has 41,000 human genes and transcripts with one 60-mer oligonucleotide probe representing each sequence. Additionally, 75 selected probes are replicated 10 times to allow for intra-array reproducibility measurements. Probes designed against 10 different mRNA spike-in control transcripts are replicated 30 times on the microarray. Thus, the sequences of 60-mer oligonucleotides represent more than 41,000 genes sequences. Unfortunately, Agilent Technologies do not provide the sequence information.

In comparison with other oncogenes, little is known about the function of the EWS-Oct-4 gene product. The GBS6 cell line was established from a pelvic bone undifferentiated sarcoma with t(6;22)(p21;q12). As a first step in investigating label-free DNA microarray bioassays using a near-field scanning microwave microscope, we selected to analyze the gene expression profile of GBS6 cell line as a model system. We used Agilent human whole genome 44k array, because it has been well known that the Agilent gene expression platform provides high flexibility and sensitivity. In addition, strong correlations of log ratios are observed between Agilent microarray results and RNA-Seq. results.

2.2. Instrumentation

The detailed description of the basic operation of a NSMM is presented in our previous work (Bhushan, 2011) and schematically shown in the inset of Fig. 1. In this study, an AFM tip with a very high input impedance was used as the NSMM probe, reducing the sensitivity of the reflection coefficient measurement. Thus, in order to boost the sensitivity of the probe, we employed a dielectric resonator and tuned the resonance cavity to match the impedance of 50 Ω of the microwave input line, so as to avoid stray contributions to the reflection coefficient. The gold and chromium coated commercial triangular AFM probe tip cantilever was directly soldered to the outside end of the coupling loop of the resonator. The free, sharp end of the tip was in close proximity to the sample surface, and was fixed at about 10 nm by using a quartz tuning fork feedback control system. The length, width, and thickness of the cantilever were 290 μm, 40 μm, and 1 μm

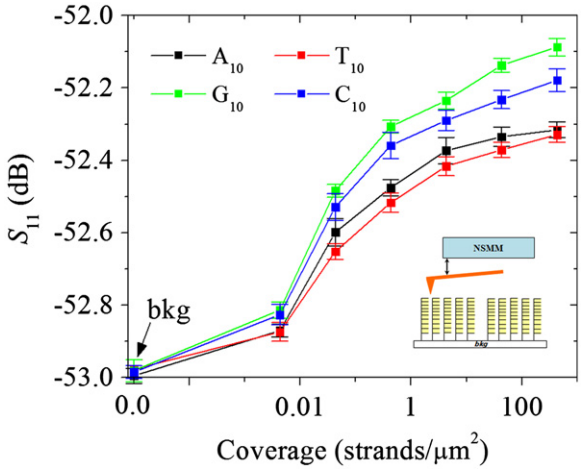

Fig. 1. The change in the microwave reflection coefficient, ΔS_{11}, as a function of coverage of 10 mer A, G, T, and C probes. The inset shows the schematic picture of oligonucleotide probes and the NSMM tip.

respectively. The apex angle of the tip was 30° and the height was about 20 μm, with a tip curvature radius of less than 40 nm. We measured the reflection coefficient S_{11} of the NSMM resonator at an operating frequency of about 3.98 GHz for the TE_{010} mode. Microwaves were generated by a network analyzer source and were input into the three-port cavity with the dielectric resonator inside. The cavity and resonator store electromagnetic energy with the resonant frequency depending strongly on material properties. In particular, the resonant frequency is sensitive to the near-field interaction of the probe tip with the sample. As the probe-sample interaction changes (e.g. due to changes of material characteristics of the sample), the coupled dipoles generate a large change in the electromagnetic energy in the resonator. Dielectric permittivity changes in the sample will cause changes of both the central resonance frequency f_r and the quality factor Q of the resonator. Therefore, by measuring the resonance frequency shift $\Delta f/f_r$ and the reflection coefficient change ΔS_{11} of the microwaves input into the cavity it is possible to monitor the dielectric permittivity of the sample. In order to optimize measurement sensitivity, both the quality of the resonator and the sensitivity of the probe must be maximized and matched; as a result, contrast of a NSMM image mainly depends on the interaction between the probe tip and the sample (Ohtsu, 1998). To extract quantitative information, it is essential to precisely control the probe tip-sample separation due to its strong influence on S_{11}.

3. Results and discussion

3.1. Microwave reflection

The resonance frequency, f_r and reflection coefficient, S_{11} changes are related to the stored electric and magnetic energies in the original and perturbed cavity, so that the shift in resonant frequency can be related to the changes in stored energy of the perturbed cavity. In addition, the magnitude of the reflection coefficient S_{11} depends on the impedance of the sample surface. Minimization of the reflection coefficient without sample is the analog of subtracting the background level in the measurement. A change in probe-sample interactions, due to variation of material characteristics of the sample, perturbs the resonance condition and changes S_{11}. Thus, the shift of resonance frequency and the change in reflection coefficient correlate with the effective intrinsic impedance of the material. A change in tip-sample interactions perturbs the system from the reference state and results in an increase in the reflectivity S_{11}.

An expression for how the reflectivity S_{11} depends on sample impedance can be derived by using standard transmission line theory (Pozar, 1990):

$$S_{11} = 20\log\left|\frac{Z_{in}-Z_0}{Z_{in}+Z_0}\right| \tag{1}$$

here Z_0 is the effective impedance of the probe tip and Z_{in} is the complex intrinsic impedance of the DNA/substrate system which can be estimated by the plane-wave solution as:

$$Z_{in} = Z_{DNA}\frac{Z_{sub}+jZ_{DNA}\tan(k_{DNA}t_{DNA})}{Z_{DNA}+jZ_{sub}\tan(k_{DNA}t_{DNA})}, \tag{2}$$

where Z_{DNA}, k_{DNA}, and t_{DNA} are the intrinsic impedance, wave number, and thickness of the DNA thin film, respectively, and Z_{sub} is the effective complex impedance of the substrate (this is similar to a dielectric on perfect metal (Al) system (Silva et al., 1996)) and it can be expressed as:

$$Z_{sub} = jZ_g k_g t_g = j\frac{Z_a}{\sqrt{\varepsilon_g\mu_g}}k_a\sqrt{\varepsilon_g\mu_g}\,t_g \cong jZ_a k_a t_g \tag{3}$$

here ε_g and μ_g are respectively the relative dielectric permittivity and the relative magnetic permeability of the glass substrate. Note that the changes of plane waves due to passing the space between the probe and sample (air environment inside cavity sensor) were neglected.

The complex input impedance of the sample can then be estimated as:

$$\begin{aligned} Z_{in} &\approx \frac{Z_a}{\sqrt{\varepsilon_g}}\frac{jZ_a k_a t_g + j(Z_a/\sqrt{\varepsilon_{DNA}})k_a\sqrt{\varepsilon_{DNA}}t_{DNA}}{(Z_a/\sqrt{\varepsilon_g}) - Z_a k_a t_g(k_a\sqrt{\varepsilon_{DNA}}/Z_a/\sqrt{\varepsilon_{DNA}})t_{DNA}} \\ &\cong j\frac{Z_a k_a(t_g+t_{DNA})}{1-k_a^2 t_g t_{DNA}\varepsilon_{DNA}} \end{aligned} \tag{4}$$

where Z_a and k_a are respectively the characteristic impedance and wave number of free-space, t_g is the thickness of the glass slide and ε_{DNA} is the relative dielectric permittivity of DNA. Thus, the microwave reflection coefficient, S_{11} is affected by the relative dielectric permittivity of DNA.

3.2. Structure analysis

Connecting the reflectivity S_{11} to molecular organization of the surface is challenging. Conceptually, one could appeal to the model of dielectric properties of DNA as proposed by (Oosawa (1971). In Oosawa's model, a single DNA chain is treated as a sphere consisting of interpenetrating positive and negative charge, with overall charge neutrality. By considering fluctuations of the dipole moment in equilibrium it is easy to calculate that the relative shift in the dielectric permittivity, $(\varepsilon-\varepsilon_0)/\varepsilon_0 \sim v\,n$ where v is the volume of a single DNA molecule and n is the coverage (concentration) of molecules. However, this spherical geometry is not very realistic. A more realistic model, also proposed by Oosawa consists of a positively charged ellipsoid with an interpenetrating ellipsoid of negative charge. While such models might provide crude approximations, they are not able to quantitatively predict the diagnostic performance of NSMM imaging. Therefore, dynamic range and sensitivity were instead considered through experimental analysis of calibration samples.

3.3. NSMM imaging: 10-mer oligonucleotides

In order to determine measurement sensitivity, experiments were designed to assess the linear dynamic range for 10-mer

homo-oligonucleotides of A, G, T, and C spotted with concentrations from 0.005 to 500 strands/μm^2 using 10-fold serial dilutions. Fig. 1 shows that the microwave reflection coefficient, S_{11}, measured at the fixed resonant frequency f_r=3.9 GHz varies nonlinearly with DNA coverage and then begins to flatten out as the response saturates at high coverages. Note that the saturation occurs without exploiting the full dynamic range of the scanner; therefore, it seems likely that it reflects diminishing per strand contributions to the signal at high coverages. The slope $d\log S_{11}(dB)/d\log\sigma$ decreases approximately 5-fold over the measured range in coverage σ. While NSMM can monitor variations in strand coverage over at least four decades, the non-linearity would need to be calibrated for quantitative coverage determination over multiple decades. The technique has excellent sensitivity for a label free method, with smallest detectable limit below 0.01 strands/μm^2 based on Fig. 1 data. This is comparable with commercial fluorescence-based scanners used in microarray applications, whose detection limit is typically within 0.1–0.05 fluorophores/μm^2 (Basarsky et al., 2000). The above estimates show that label-free NSMM detection can approach if not exceed the sensitivity of conventional fluorescence diagnostics.

Fig. 2 shows the 2D NSMM images of the 10-mer data for A, G, T, and C probes. The insets show the cross-sectional presentations along the gray line. From the data, relative to the aminosilanized glass as reference, the reflection coefficient change for the lowest coverage specimens for A_{10}, G_{10}, T_{10}, and C_{10} was 0.09, 0.18, 0.11, and 0.21 dB compared to 0.79, 1.03, 0.71, and 0.93 dB for the highest coverages spots, respectively. The data also suggest that certain bases contribute more to the NSMM signal; e.g. that G engenders a stronger interaction with the tip than A or T. While such base-specific differences would not be unexpected, their interpretation in terms of molecular characteristics (e.g. polarizability) would be premature without additional details on the surface environment. For example water of hydration, base orientation and stacking, and uniformity of strand coverage could vary depending on base type and contribute to differences in the NSMM signal that may or may not extrapolate well to mixed base sequences. Such various possible contributions to S_{11}, representing important but difficult-to-track aspects of surface modification with DNA molecules, merit a more detailed study separate from the current focus on the NSMM technique. However, changes in S_{11} intensity variation with strand coverage were clearly visible for all four base types down to ~0.01 strands/μm^2.

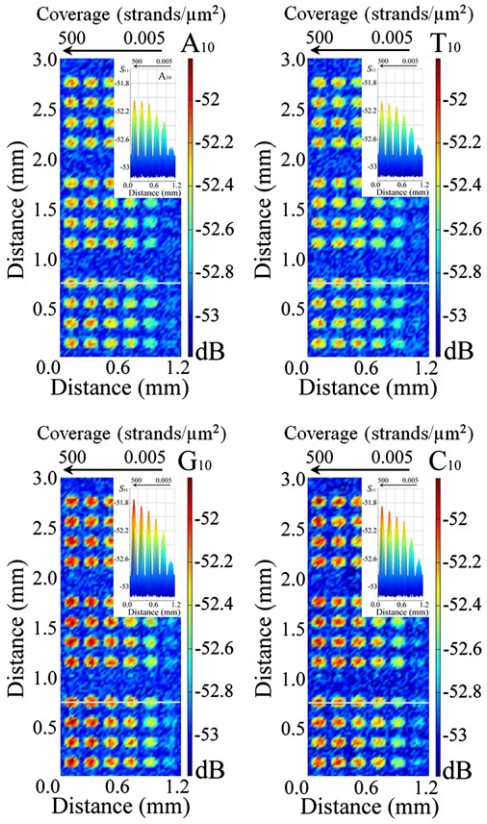

Fig. 2. 2D NSMM images of the 10-mer data for A, G, T, and C probes. The insets show the cross sectional profiles indicated by the solid line.

3.4. NSMM imaging: 60-mer oligonucleotides

Fig. 3 shows a 3D NSMM image of an unhybridized Agilent 60-mer oligonucleotide microarray for a scan area of about 200 × 200 μm^2 with 2 μm resolution. Ordered oligonucleotide probe elements, approximately 60 μm in diameter, are surrounded by areas of silanized glass substrate. The microwave images showed clear contrast between the oligonucleotide probe spots and the surrounding background regions, where a sharp contrast in "height" was observed due to the relative dielectric permittivity changes. The corresponding cross sectional scan better indicates the contrast in signal between the probes and the unmodified regions as shown in the inset of Fig. 3. This result demonstrates that NSMM can be used for quality characterization of commercial microarrays; for example, to provide an indication of probe spot uniformity and reproducibility in probe density from spot to spot. A key benefit of NSMM is that contrast is provided by physical properties (relative permittivity variations) as visualized in the microwave range, so that NSMM can be applied to the characterization of microarray features directly, without extraneous labels such as fluorophores. Label-free imaging can be also performed by other high-resolution analytical detection techniques such as atomic force microscopy (Mizuno et al., 2004; Oliveira Brett and Chiorcea Paquim, 2005; Lyubchenko, 2011), that can in principle similarly provide information on topography, uniformity, and quality. However, even for such state of the art tools, surface features can be difficult to resolve against the background of silanized glass if the background is not flat and does not possess sufficient contrast in mechanical properties. The outstanding sensitivity of NSMM to local variations in relative permittivity may therefore prove very fruitful for assessing probe spot uniformity and molecular coverages in DNA as well as other microarrayed platforms.

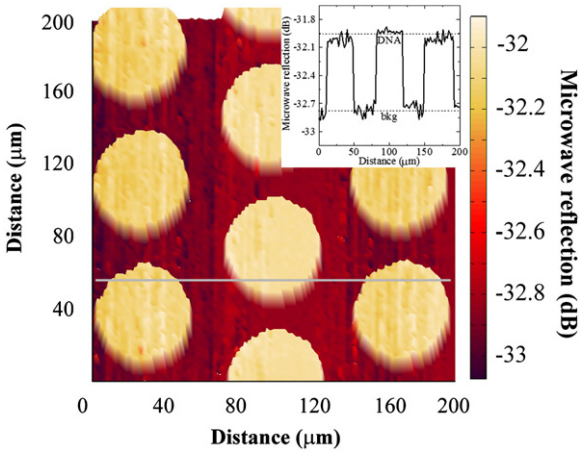

Fig. 3. 3D NSMM image of unhybridized 60-mer probe Agilent 44k DNA microarray. Image area was 200 × 200 μm^2 and scanning resolution was 2 μm. The inset shows the cross sectional profile indicated by the solid line in the 3D NSMM image.

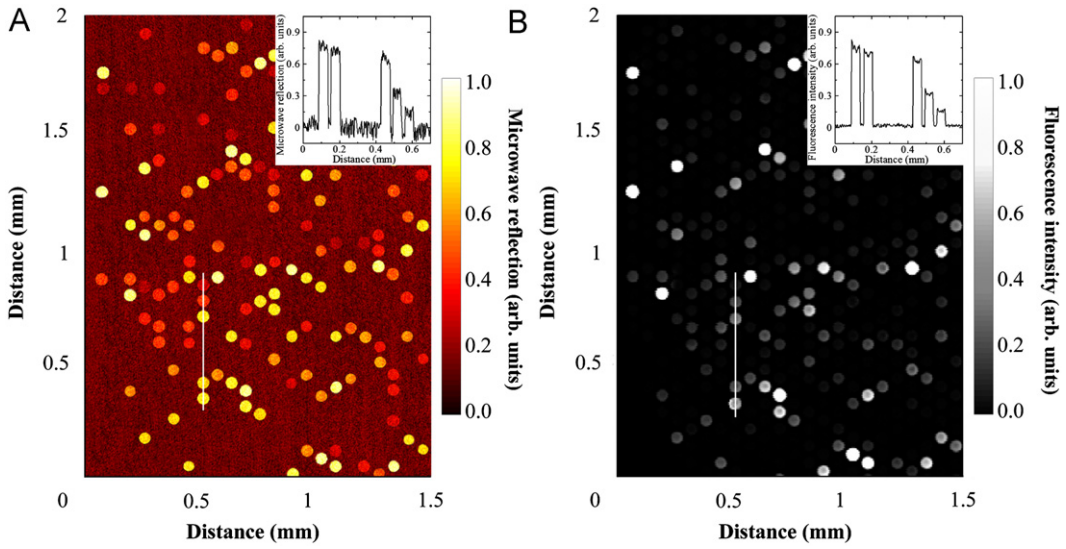

Fig. 4. (a) 2D NSMM map (with 2 μm scanning resolution) and (b) fluorescence image (prepared by Agilent Technologies) of the hybridized 60-mer DNA microarray. The same position with 1.5×2 mm^2 surface area of the microarray is shown in both images. The insets show the corresponding cross sectional profiles along the solid lines in each image.

3.5. Microarray 3D mapping: NSMM and fluorescence images

A major motivation for the present study was to compare NSMM label-free detection of hybridization with that of conventional commercial hardware. This was done by comparing NSMM images with those obtained with the Agilent microarray scanner, using 60-mer oligonucleotide Agilent 44 k microarrays hybridized to complex human targets as described in the experimental section. A series of experiments were performed (independent trials for over 140 spots) to examine the correlation between the two imaging techniques. Fig. 4(a and b) respectively shows an NSMM image and fluorescence image prepared by the Agilent scanner, on the same position with the scan area of 1.5×2 mm^2. The observed intensity gradation between microwave signal and luminescence intensity shows very similar behavior. This similarity is further highlighted in the insets of Fig. 4 which show cross sectional line scan intensity profiles of NSMM and fluorescence images along the solid lines indicated on 2D images. Good correlation is again evident between the two imaging techniques. The line scan intensity measurements also show good contrast in signal between the hybridized spots compared to the surrounding background. The obtained microarray spot diameters for both unhybridized and hybridized probe spots were about 60 μm and agree well. Thus, the NSMM can quantify hybridization processes while providing images with high scanning resolution and intensity (Melikyan et al., 2009).

For each NSMM spot in Fig. 4(a), the S_{11} raw data consist of approximately 335 values in the x and y directions which can be averaged to a single number to represent the NSMM signal for that spot. Comparison of these microwave intensities with the fluorescent intensities can more directly evaluate correlation between NSMM and fluorescence images. This is considered in Fig. 5, which plots the log signal intensities for the two methods against one another. To calculate the mean log ratio, the average NSMM response (S_{11} at 3.98 GHz) for a spot was normalized by the DNA-free (i.e. salinized glass substrate) S_{11} value; these values therefore range from 0 to 1 (i.e. 0 means DNA-free and 1 means highest reflection for microwave data). The log ratio for the fluorescence data was normalized by the highest intensity of fluorescence raw data taken from images in Fig. 4. Fig. 5 shows that the two techniques show a high correlation coefficient $R^2 = 0.9923$. Therefore, despite an entirely label-free mechanism

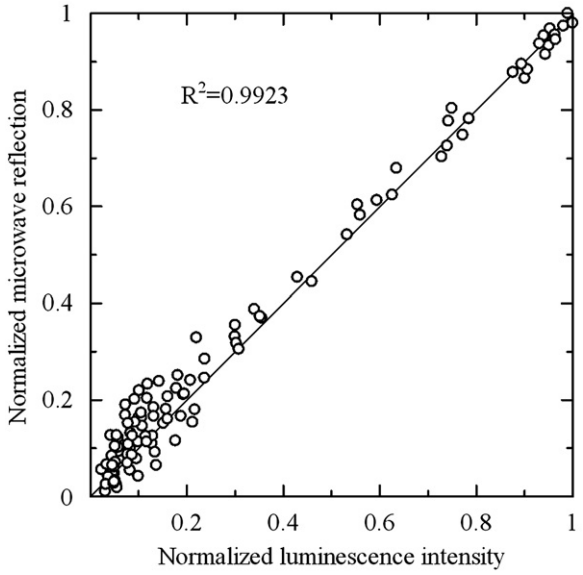

Fig. 5. Correlation of the normalized microwave reflection coefficient with fluorescence amplitude for spots in the hybridized Agilent 44k microarray. S_{11} was normalized to the slide substrate as background, while fluorescence intensity was normalized to the highest measured signal.

of contrast, NSMM can characterize the hybridized state of a microarray comparably to conventional label-based, fluorescence protocols. NSMM scan field is relatively uniform across the entire slide and varies with a pixel standard deviation of less than 2.7% and correlation coefficient over 0.9923 for the 60-mer nucleotide which is of order the errors and correlation value obtained by Agilent; about 2% and 0.9901 for a 25-mer nucleotide (Corson et al., 2004).

4. Conclusions

The main advantage of NSMM over other label-free detection methods is its outstanding sensitivity and high scanning resolution (potentially less than 50 nm). As a label-free method, NSMM readout does not require labeling of target sequences with

fluorophores or other tagging groups. Although the mechanism of contrast, derived from differences in relative permittivity at GHz frequencies, is not entirely understood in terms of contributions from DNA sequence, conformation, and complexation (e.g. with water), the results presented demonstrate good correlation between this signal and that obtained fluorescently from the same hybridized microarray. Moreover, NSMM could be used to image microarrays before hybridization to confirm quality of manufacture and to flag any defective spots. These advantages render NSMM as a sensitive and flexible tool for DNA as well as other microarray applications. The above estimates show that even when multiple fluorophores are used per strand, label-free NSMM detection can approach if not exceed the sensitivity of conventional fluorescence diagnostics. Label-free operation is especially attractive as it avoids the costs, sample variability, and delays associated with fluorescent or other tagging. Future advances will focus on decreasing of mapping time and total noise factor to improve the contrast and resolution.

Acknowledgments

This work was supported by a Sogang University Special Research Grant 2012 (201214003), the Basic Science Research Program through the National Research Foundation of Korea (2012–0002250), Priority Research Centers Program through the National Research Foundation of Korea (2012–0006690), Parts and Materials International Collaborative R&D Program (MKE, Korea; N0000481), and MEST and PAL (Korea). R.L. and S.K. acknowledge support from the National Institutes of Health of the USA (NHGRI R33HG003089).

We thank Dr. Takuro Nakamura (Japanese Foundation for Cancer Research) for providing GBS6 cell line.

References

Abu-Teir, M., Golosovsky, M., Davidov, D., Frenkel, A., Goldberger, H., 2001. Review of Scientific Instruments 72, 2073–2079.
Basarsky, T., Verdnik, D., Zhai, J.Y., Wellis, D., 2000. In: Schena, M. (Ed.), Microarray Biochip Technology. Eaton Publishing, Natick, MA, pp. 265–284.
Baur, J., Gondran, Ch., Holzinger, M., Defrancq, E., Perrot, H., Cosnier, S., 2010. Analytical Chemistry 82, 1066–1072.
Bhushan, B., 2011. Scanning probe microscopy in nanoscience and nanotechnology 2. Springer, Berlin.
Cao, Ch., Kim, J.H., Yoon, D., Hwang, E.-S., Kim, Y.-J., Baik, S., 2008. Materials Chemistry and Physics 112, 738–741.
Corson, J.F., Delenstarr, G., Collins, P.J., Doan, T.B., McMillan, J.M., 2004. Agilent Technologies, 5988–9498EN.
Dolatabadi, J.E.N., Mashinchian, O., Ayoubi, B., Jamali, A.A., Mobed, A., Losic, D., Omidi, Y., de la Guardia, M., 2011. Trends in Analytical Chemistry 30, 459–472.
Elson, E., 2007. Progress in Biophysics & Molecular Biology 95, 1–15.
Friedman, B., Gaspar, M.A., Kalachikov, S., Lee, K., Levicky, R., Shen, G., Yoo, H., 2005. Journal of the American Chemical Society 127, 9666–9667.
Hanai, T., Hamada, H., Okamoto, M., 2006. Journal of Bioscience and Bioengineering 101, 377–384.
Kim, J., Kim, M., Lee, K., Lee, J., Cha, D., Friedman, B., 2003. Measurement Science & Technology 14, 7–12.
Kim, S., Jang, Y., Kim, S., Kim, T.-D., Melikyan, H., Babajanyan, A., Lee, K., Friedman, B., 2011. Journal of Nanoscience and Nanotechnology 11, 4222–4226.
Knoll, B., Keilmann, F., Kramer, A., Guckenberger, R., 1997. Applied Physics Letters 70, 2667–2669.
Lamartine, J., 2006. Materials Science and Engineering: C 26, 354–359.
Lim, E., Manaka, T., Iwamoto, M., Friedman, B., Babajanyan, A., Kim, S., Yoon, Y., Kim, S., Lee, K., 2008. Thin Solid Films 516, 2573–2576.
Lin, Ch.-H., Hung, Ch.-H., Hsiao, Ch.-Y., Lin, H.-Ch., Ko, F.-H., Yang, Y.-Sh, 2009. Biosensors & Bioelectronics 24, 3019–3024.
Lyubchenko, Y.L., 2011. Micron 42, 196–206.
Maruyama, Y., Terao, S., Sawad, K., 2009. Biosensors & Bioelectronics 24, 3108–3112.
Melikyan, H., Sargsyan, T., Babajanyan, A., Kim, S., Kim, J., Lee, K., Friedman, B., 2009. Journal of Magnetism and Magnetic Materials 321, 2483–2787.
Mizuno, R., Haruta, H., Morii, T., Okada, T., Asakawa, T., Hayashi, K., 2004. Thin Solid Films 464–465, 459–463.
Ohtsu, M., 1998. Near-Field Nano/Atom Optics and Technology. Springer, Tokyo.
Oliveira Brett, A.M., Chiorcea Paquim, A.M., 2005. Bioelectrochemistry 66, 117–124.
Oosawa, F., 1971. Polyelectrolytes. Marcel Dekker, New York.
Ozkumur, E., Ahn, S., Yalcin, A., Lopez, C.A., Cevik, E., Irani, R.J., DeLisi, Ch., Chiari, M., Unlu, M.S., 2010. Biosensors & Bioelectronics 25, 1789–1795.
Pei, R., Cheng, Z., Wang, E., Yang, X., 2001. Biosensors & Bioelectronics 16, 355–361.
Postma, H.W.Ch., 2010. Nano Letters 10, 420–425.
Pozar, D., 1990. Microwave Engineering. Addison-Wesley, New York.
Qi, Y., Li, B., Zhang, Zh., 2009. Biosensors & Bioelectronics 24, 3581–3586.
Ray, K., Ma, J., Oram, M., Lakowicz, J.R., Black, L.W., 2010. Journal of Molecular Biology 395, 1102–1113.
Ryu, S.-W., Kim, Ch.-H., Han, J.-W., Kim, Ch.-J., Jung, Ch., Park, H.G., Choi, Y.-K., 2010. Biosensors & Bioelectronics 25, 2182–2185.
Shervedani, R.K., Mehrjardi, A.H., Zamiri, N., 2006. Bioelectrochemistry 69, 201–208.
Silva, E., Lanucara, M., Marcon, R., 1996. Superconductor Science and Technology 9, 934–941.
Son, A., Dosev, D., Nichkova, M., Ma, Zh., Kennedy, I.M., Scow, K.M., Hristova, K.R., 2007. Analytical Biochemistry 370, 186–194.
Van Schothorst, E.M., Pagmantidis, V., de Boer, V.C.J., Hesketh, J., Keijer, J., 2007. Analytical Biochemistry 363, 315–317.
Wang, L., Li, P.C.H., 2011. Analytica Chimica Acta 687, 12–27.
Zhang, D., Peng, Y., Qi, H., Gao, Q., Zhang, C., 2010. Biosensors & Bioelectronics 25, 1088–1094.
Zheng, H., Goldner, L.S., Leuba, S.H., 2007. Methods 41, 342–352.
Zhu, N., Lin, Y., Yu, P., Su, L., Mao, L., 2009. Analytica Chimica Acta 650, 44–48.
Ziolkowski, R., Gorski, L., Zaborowski, M., Malinowska, E., 2010. Bioelectrochemistry 80, 31–37.